Human Molecular Genetics, 2023, Vol. 32, 24, 3361–3373
https://doi.org/10.1093/hmg/ddad157
Advance access publication date 21 September 2023
Original Article

Divergent phenotypes in constitutive versus conditional mutant mouse models of Sifrim-Hitz-Weiss syndrome

Sarah Larrigan[1,2], Shrilaxmi V. Joshi[1,2], Pierre Mattar[1,2,*]

[1]Ottawa Hospital Research Institute (OHRI), Ottawa, ON K1H 8L6, Canada
[2]Department of Cellular and Molecular Medicine, University of Ottawa, Ottawa, ON K1H 8M5, Canada

*Corresponding author. Department of Cellular and Molecular Medicine, University of Ottawa, Ottawa, ON, K1H 8M5, Canada. E-mail: pmattar@ohri.ca

Chromatin remodellers are among the most important risk genes associated with neurodevelopmental disorders (NDDs), however, their functions during brain development are not fully understood. Here, we focused on Sifrim-Hitz-Weiss Syndrome (SIHIWES)—an intellectual disability disorder caused by mutations in the *CHD4* chromodomain helicase gene. We utilized mouse genetics to excise the *Chd4* ATPase/helicase domain—either constitutively, or conditionally in the developing telencephalon. Conditional heterozygotes exhibited no change in cortical size and cellular composition, and had only subtle behavioral phenotypes. Telencephalon-specific conditional knockouts had marked reductions in cortical growth, reduced numbers of upper-layer neurons, and exhibited alterations in anxiety and repetitive behaviors. Despite the fact that whole-body heterozygotes exhibited comparable growth defects, they were unaffected in these behaviors, but instead exhibited female-specific alterations in learning and memory. These data reveal unexpected phenotypic divergence arising from differences in the spatiotemporal deployment of loss-of-function manipulations, underscoring the importance of context in chromatin remodeller function during neurodevelopment.

Graphical Abstract

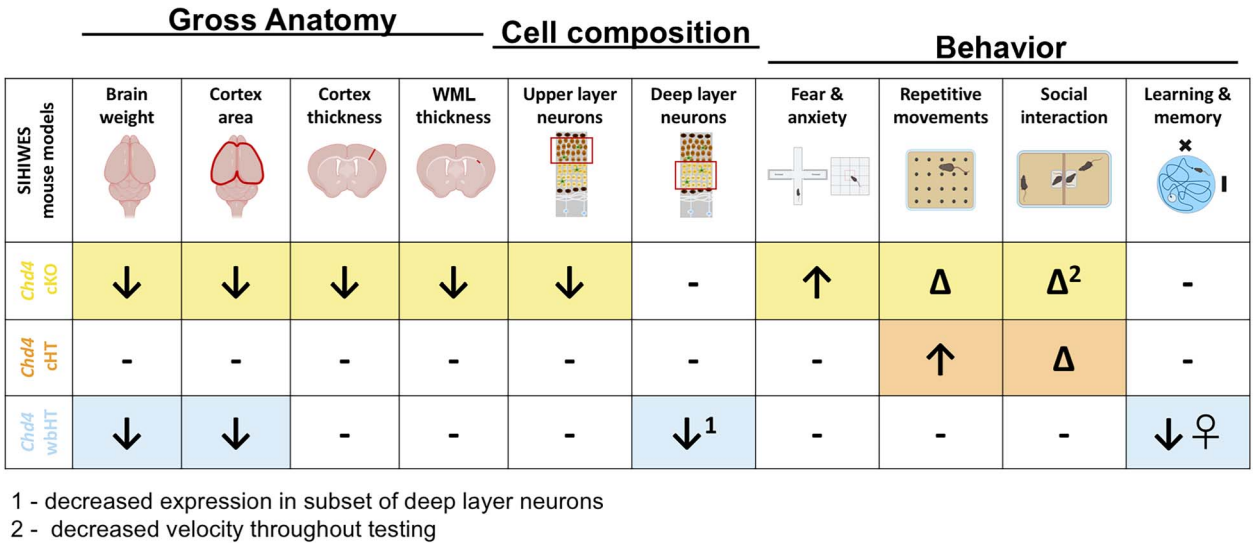

Keywords: chromatin remodelling; neurodevelopmental disorder; intellectual disability; behavior; neocortex

Introduction

The histogenesis of the central nervous system (CNS) depends upon the ordered deployment of many developmental processes, including progenitor proliferation, differentiation, migration, axon pathfinding, and synapse maturation—all of which critically depend on dynamic changes in gene expression. Chromatin remodellers mobilize nucleosomes to help reconfigure the epigenome, facilitating transitions between activated and repressed states. There are four main families of chromatin remodelling enzymes: SWI/SNF, ISWI, CHD, and INO80, each of which is encoded by multiple paralogues [1]. For example, the mammalian CHD family encompasses 10 different genes. Despite this putative redundancy, chromatin remodellers are among the most important risk genes for intellectual disability (ID) and autism spectrum disorder (ASD) [2–4], suggesting that these genes have specific neurodevelopmental functions.

Received: February 15, 2023. **Revised:** September 14, 2023. **Accepted:** September 15, 2023

Subfamily II CHD genes—consisting of *CHD3*, *CHD4*, and *CHD5*—are notable. These subunits exclusively incorporate into the nucleosome remodelling and deacetylase (NuRD) complex [5]. In addition to nucleosome remodelling activity, the NuRD complex also contains Class I histone deacetylase enzymes [6–8], and thereby functions as a critical epigenetic 'eraser'. CHD4 has been additionally shown to incorporate into a second complex called ChAHP (CHD4, ADNP, HP1) [9], which does not include histone deacetylases. Both NuRD and ChAHP complexes are associated with gene repression, heterochromatinization, and suppression of genomic accessibility [5, 9–14].

De novo variants in *CHD4* cause the overgrowth-intellectual disability syndrome (see Supplemental section for a discussion of terminology) known as Sifrim-Hitz-Weiss syndrome (SIHIWES; MIM 617159) [15–17]. 32 individuals with SIHIWES have been characterized to-date. All patients were heterozygous with nearly all variants being missense or in-frame insertions/deletions, with the exception of three variants predicted to lead to truncated proteins. Notably, the majority of the missense mutations mapped to the ATPase/helicase enzymatic domains. SIHIWES symptoms are variable in affected patients. Mild to moderate ID, macrocephaly, and delayed speech are hallmark symptoms. Additionally, 22 of the 23 individuals that underwent MRI brain imaging presented with neuroanatomical abnormalities including ventriculomegaly, hydrocephalus, Chiari 1, and corpus callosum hypoplasia. Outside of the brain, SIHIWES was also associated with hearing loss, hypotonia, motor delay, and abnormalities in the heart, skeleton, vasculature, and gonads [15–17]. These findings support the idea that CHD4 acts on basic developmental processes. Other subfamily II genes have also been linked to neurodevelopmental disorders, with variants in the *CHD5* and *CHD3* genes identified as the cause of Parenti-Mignot neurodevelopmental syndrome (MIM 619873) and Snijders Blok-Campeau syndrome (MIM 618205), respectively [18, 19].

To begin to understand the molecular mechanisms through which CHD4 contributes to neurodevelopment, a variety of animal models have previously been generated. *Chd4* is an essential gene [20, 21], necessitating conditional approaches to generate CNS knockouts. In postmitotic cerebellar neurons, conditional knockouts (cKOs) have revealed that *Chd4* plays critical roles in gene regulation and circuit function [13, 22, 23]. With respect to growth of the brain, previous work has shown that *Chd4* is required for the survival and proliferation of cortical progenitor cells during neurogenesis [24], but perinatal lethality precluded analysis of postnatal brain development and behavior. Moreover, while *CHD4* mutations associated with SIHIWES are heterozygous, the reported phenotypes in both the cerebellum and cortex were observed only in homozygous *Chd4* cKOs. Heterozygote phenotypes were not reported in the above studies.

To compare how *Chd4* knockout and/or haploinsufficiency affect neurodevelopment, we generated novel mouse models. Using the *Emx1-Cre* driver [25], we conditionally ablated *Chd4* from the developing dorsal telencephalon. Conditional heterozygotes (cHTs) and cKOs proved to be viable, permitting us to examine postnatal phenotypes. We additionally used *CMV-Cre* [26] to create whole-body heterozygotes (wbHTs). While we expected *Chd4* cHT and wbHT mice to be similar, cHT mice exhibited behavioral phenotypes related to sociability and repetitive/stereotyped behaviors. By contrast wbHT mice had significant reductions in cortical size, and divergent behavioral phenotypes related to learning and memory. Our data reveal surprising phenotypic heterogeneity arising from similar loss-of-function manipulations, underscoring the pleiotropy of chromatin remodellers in neurodevelopment.

Results

In order to assess the role of *Chd4* in neurodevelopment and behavior, we began by examining Chd4 expression. In accordance with previous reports [24], we found that Chd4 protein was expressed in a widespread fashion throughout cortical development—both in dividing progenitor cells, and in differentiated neurons and glia (Fig. S1).

As most patients with SIHIWES harbor mutations in the SNF2-like domains of *CHD4*, we took advantage of a previously developed mouse line that allows for excision of the *Chd4* ATPase/helicase domain using a Cre/loxp approach [21]. We utilized *Emx1-Cre* [25] to ablate *Chd4* in the developing dorsal telencephalon, generating cHTs and cKOs. We additionally used *CMV-Cre* [26] to ablate *Chd4* throughout the body, generating wbHTs (Fig. 1A). To validate the conditional genetics strategy as well as our Chd4 immunohistochemistry, we first examined Chd4 protein expression using 3 antibodies, 2 of which were raised against epitopes mapping outside of the floxed ATPase domain. Staining revealed that Chd4 protein was completely lost in the embryonic *Chd4* cKO neocortex as expected (Fig. 1B and C, see also Fig. S4).

Chd4 is required for cortical growth

Chd4 cKOs had previously been generated using the *Nestin-Cre* driver allele, but were reported to be perinatally lethal [24]. We reasoned that the later onset and more spatially restricted expression of the *Emx1-Cre* driver might improve the survival of cKOs. Indeed, we were able to successfully generate adult *Chd4* cKOs. However, we found that they were not recovered in Mendelian frequencies suggesting considerable developmental lethality (Table 1). *Chd4* wbHT mice were born in normal Mendelian ratios.

Next, we measured brain sizes and weights at postnatal day (P) 7. Grossly, we found that *Chd4* cKOs had a marked reduction in the size of the dorsal telencephalon (Fig. 2A). Brain weight was accordingly reduced in cKO animals (Fig. 2B). *Chd4* wbHTs had a small but significant reduction in brain weight (Fig. 2B). Similar differences were observed in cortical area—measured by manually tracing the telencephalic hemispheres in two-dimensional images (Fig. 2C, Fig. S2). To determine whether these growth defects were specific to the cortex, we performed similar area measurements of the cerebellum. We found no difference in cHT and cKO cerebellar area, in accordance with the lack of *Emx1-Cre* expression in this territory [25]. The wbHT cerebellum area was likewise unaffected despite body-wide heterozygosity (Fig. 2D). As an additional control, we measured animal body weights. We found no significant difference between control, cHT, and cKO animals. The body weights of wbHT animals were slightly but significantly reduced vs. wild-type controls (Fig. 2E). Both males and females appeared to be equivalently affected (Fig. S3). Thus, we find that *Chd4* is required for cortical growth, as was previously described by the Riccio laboratory [24]. Interestingly, in the hemizygous condition, *Chd4* can also lead to cortical hypoplasia when deleted constitutively, but not when deleted conditionally at the onset of neurogenesis.

To determine how the gross changes in cortical size relate to cellular composition, we next examined P7 brains histologically, focusing on the somatosensory cortex. At this stage, all neocortical projection neurons have been generated, and have taken up their positions in the cortical plate. We first performed immunohistochemistry for Chd4 in coronal tissue sections. As per embryonic stages (Fig. 1C), Chd4 protein expression was markedly reduced in the *Chd4* cKO (Fig. S4A). Although residual Chd4 protein remained expressed, the observed pattern was consistent with

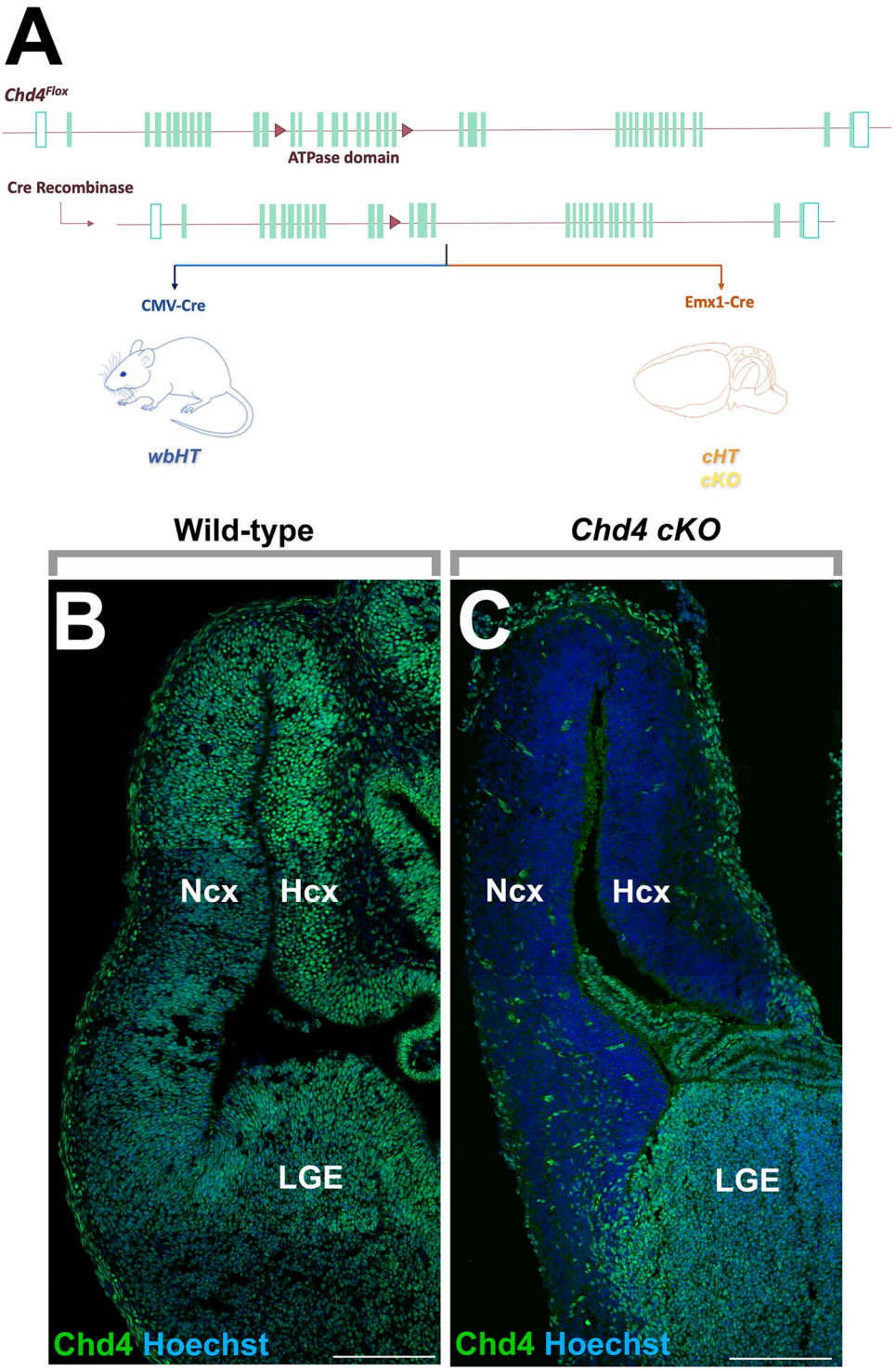

Figure 1. *Chd4* conditional and constitutive mutants. (A) Genetic strategies for generating whole-body heterozygotes (wbHTs), as well as telencephalon-specific $Chd4^{Fl/+}$ conditional heterozygotes (cHTs) and $Chd4^{Fl/Fl}$ conditional knockouts (cKOs). The $Chd4^{Fl}$ allele has loxP sites flanking exons 12 to 21, encompassing the ATPase domain [21]. (B, C) Chd4 immunohistochemistry on coronal sections from E13.5 wild-type (B) and cKO (C) forebrains. Ncx: neocortex, Hcx: hippocampus; LGE: lateral ganglionic eminence. Scale bar = 200 μm.

expression from inhibitory interneurons and endothelial cells that are outside the *Emx1-Cre* lineage. Chd4 protein expression in cHT and wbHT brains was not obviously different versus controls (Fig. S4A).

We next measured the thickness of the neocortical layers. In accordance with the gross reduction in cortical size observed in *Chd4* cKOs, we found that the thickness of the neuronal layers was significantly reduced (Fig. S4B). Likewise, the thickness of the white matter layer was significantly reduced in cKOs (Fig. S4C). Conversely, cHT and wbHT neocortices were not different from controls. Next, we performed cell counts. We quantitated Hoechst+ nuclei in 200 μm-wide columns of the somatosensory cortex, which revealed decreases in absolute cell numbers in cKOs (Fig. S4D), and no change in cHT or wbHT cell

Table 1. Postnatal survival of *Chd4* cHT and cKO mice.

Emx1-Cre+; Chd4$^{fl/+}$ x *Chd4*$^{fl/fl}$	*Chd4*$^{fl/fl}$		*Chd4*$^{fl/+1}$	
	Emx1-Cre-	*Emx1-Cre+*	*Emx1-Cre-*	*Emx1-Cre+*
Expected	19.25	19.25	19.25	19.25
Observed	34	3	14	26
Chi-square value	11.30195	13.71753	1.431818	2.366883
Probability	0.05*	0.01**	n.s.	n.s.

Emx1-Cre+; Chd4$^{fl/+}$ mice were crossed with *Chd4*$^{fl/fl}$ mice to yield *Chd4* cHTs and cKOs. Litters were collected between P7 and P21 (77 pups total). Probability based off chi-square value was calculated. Degrees of freedom = 3. *$p < 0.05$; **$p < 0.01$.

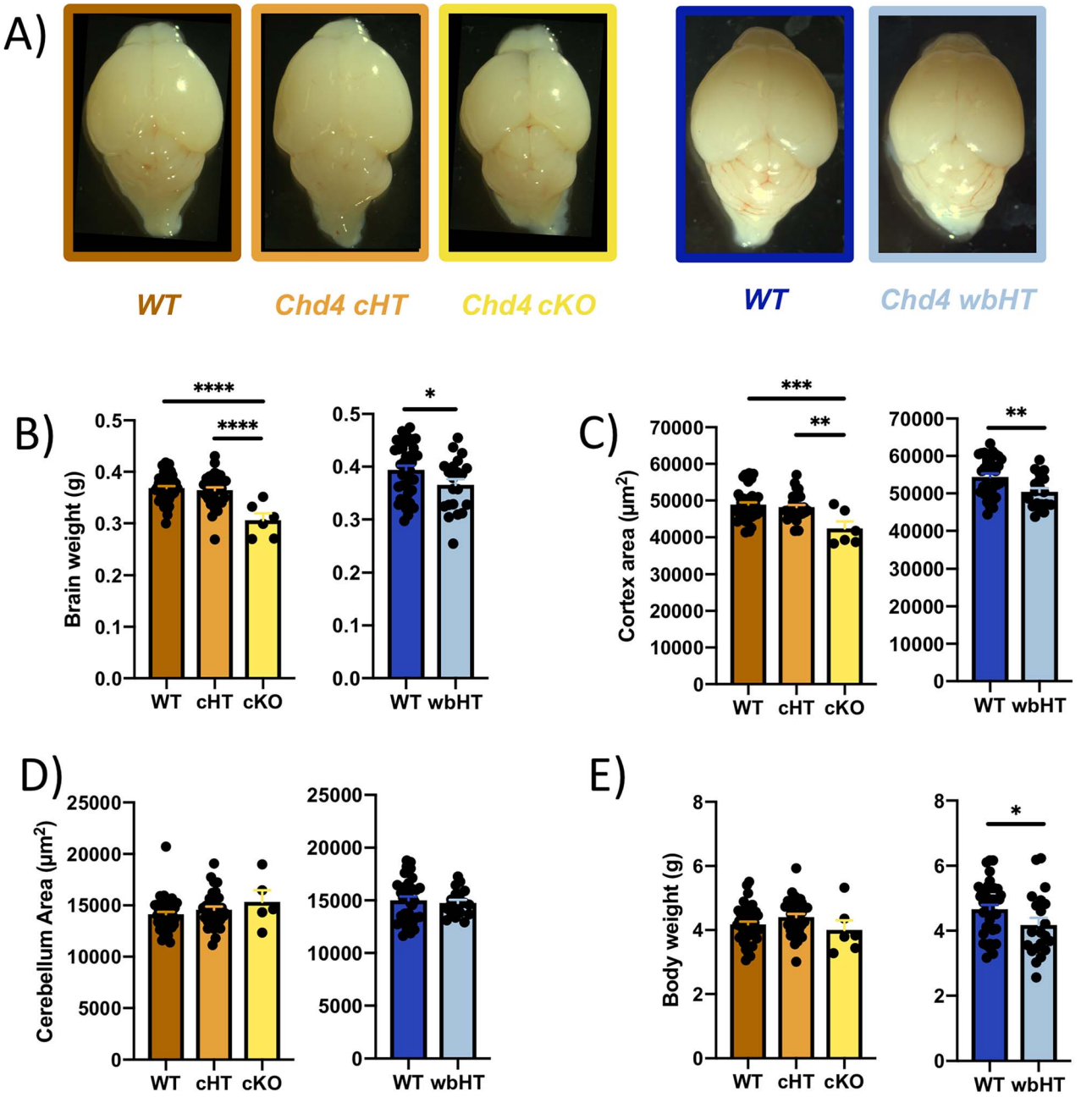

Figure 2. *Chd4* is required for cortical growth. (A) Wholemount images of wild-type, cHT, cKO, and wbHT brains harvested at P7. (B–E) P7 size measurements according to genotype as indicated. (B) Brain weight. *Emx1-Cre* line: wild-type n = 46, cHT n = 34, cKO n = 6. *CMV-Cre* line: wild-type n = 39, wbHT n = 21. (C) Cortex area. au: arbitrary units. *Emx1-Cre* line: wild-type n = 46, cHT n = 34, cKO n = 6. *CMV-Cre* line: wild-type n = 33, wbHT n = 19. (D) Cerebellum area. *Emx1-Cre* line: wild-type n = 44, cHT n = 32, cKO n = 5. *CMV-Cre* line: wild-type n = 32, wbHT n = 19. (E). Body weight. *Emx1-Cre* line: wild-type n = 46, cHT n = 34, cKO n = 6. *CMV-Cre* line: wildtype n = 39, wbHT n = 21. Statistical analyses for wild-type, cHT, and cKO comparisons are via one-way ANOVA with the Tukey-Kramer post-hoc test. Comparisons of wild-type vs. wbHT are via Student's t-test. See also Supplemental Data File for statistical summary. *$p < 0.05$; **$p < 0.01$; ****$p < 0.0001$.

numbers. Moreover, there were no changes in cell density in any of the genotypes (Fig. S4E). Next, we divided the neuronal layers into 6 equally sized bins. We found that *Chd4* cKOs exhibited a proportionate reduction in cells within bin 2 (Fig. S4F), which generally maps to the upper layers of the cortex (see diagram in Fig. S4A). Cell counts in wbHT neocortices were proportionately reduced in 2 out of 6 bins (Fig. S4F), perhaps reflecting the decrease in gross cortical size observed previously in wholemount (Fig. 2A and B).

Next, we examined cell-type specific marker proteins. We examined markers for lower layer (Ctip2 and Tbr1) and upper-layer (Brn2 and Satb2) neuronal subtypes (Fig. S5A). We again counted absolute cell numbers within 200 μm-wide columns, and proportionate cell numbers by dividing the neuronal layers into 6 equally-sized bins as per above. In accordance with a previous study [24], we found that cKOs exhibited a significant reduction in upper-layer neurons—marked both by Brn2+ and Satb2+ (Fig. S5B and C). We found that early born lower-layer cortical neurons, marked by Ctip2 and Tbr1, were not affected in cHTs and cKOs (Fig. S5D and E). However, we observed a significant reduction in Ctip2+ neurons in wbHT neocortices (Fig. S5D). Ctip2 expression is most prominent in Layer V, but we did not observe a difference in proportions of Ctip2+ cells in the corresponding bin (bin 5). Instead, reductions were most apparent in the most basal bin 6, as well as in the most apical bins 1 and 2 (Fig. S5D), where Ctip2 is normally expressed at low levels. Moreover, these changes were not matched by changes in Tbr1+ cell numbers (Fig. S5E). These data suggest that the observed changes in Ctip2 expression are likely due to alterations in Ctip2 expression levels rather than changes in cell numbers. Finally, we measured glial cell numbers, but observed no differences in overall numbers of Olig2+ oligodendrocyte-lineage cells, or in Aldh1l1+ astrocytes (Fig. S6). Together, these data suggest that *Chd4* is specifically required for the expansion of late-born cortical neurons, and suggest that constitutive *Chd4* haploinsufficiency may additionally affect Ctip2 expression.

Assessing activity and anxiety levels in *Chd4* mutants

To determine how the observed anatomical changes correlated with behavioral defects, we ran mutant mice through a battery of tests. We chose to assess *CMV-Cre* and *Emx1-Cre* lines independently due to subtle but significant differences observed in the baseline behavior of the control mice. We examined sexes separately, but generally found few differences and therefore pooled male and female data together in order to increase statistical power. However, we present sex-specific data where significant differences were observed.

As many of our behavioral tests depend on vision, we tested the optokinetic reflex of mutant mice, but observed no differences versus controls (Fig. S7). We measured circadian activity levels using the beam break test, in which mice are placed in a cage containing an array of photobeams. The ambulatory movement of mice within the cage leads to beam interruptions that are tabulated over the course of 24 h. We observed little difference in the circadian activity levels of *Chd4* cHT, cKO, or wbHT mice versus controls (Fig. 3A and B).

Having found no major differences in gross sensorimotor behavior, we examined mutant mice in the open field test, which assesses activity levels and anxiety. Animals are placed in a square-shaped arena with brighter illumination at the center. Mice are normally light-aversive, and spend more time in the darker corners of the chamber. We observed that *Chd4* cKOs spent more time in the open central area of the testing arena (Fig. 3C). *Chd4* cHT and wbHT mice did not exhibit differences versus controls. Upon further examination, we determined that the *Chd4* cKO phenotype arises due to the fact that the mice 'freeze' upon being placed in the brightly lit center of the testing arena, leading to increased latency to reach the corners. While overall velocity levels were not affected (Fig. 3H), *Chd4* cKOs exhibited reduced velocity specifically within the first minute of testing (Fig. 3I), after which, their activity patterns were indistinguishable from controls (see Fig. S8). These data suggest that *Chd4* cKO mice may experience elevated anxiety upon encountering a novel environment.

In contrast, we observed a different phenotype in the elevated plus maze test—which also tests for fear/anxiety. Mice are placed in a 'plus symbol' -shaped maze containing two walled arms and two open arms. Mice typically prefer the more sheltered closed arms of the maze, and avoid the open arms and the central zone. In this test, *Chd4* cKO, cHT and wbHT mice did not differ from controls (Fig. 3J–P). Taken together, these results suggest that *Chd4* cKOs may present with elevated anxiety levels in certain novel and/or open environments, which is best captured in the open field test, and not in others (elevated plus maze).

Assessing social and repetitive behaviors in *Chd4* mutants

We performed behavioral testing for social and repetitive behaviors, which are often affected in mouse NDD models. We performed the adult social interaction test, in which a mouse is first habituated to a chamber within an empty cage, and subsequently reintroduced into the cage with a stranger mouse placed into the chamber. *Chd4* cKOs exhibited marked behavioral differences, although they likely do not reflect a phenotype in sociability. When partner mice were placed in the interaction chamber, we found that *Chd4* cHT, cKO, and wbHT mice spent more time in the interaction zone of the testing arena as expected (Fig. 4A and B). However, *Chd4* cKOs entered the socialization areas significantly less frequently. Importantly, the same effect occurred during the habituation phase, when the interaction partner mouse was absent (Fig. 4A and B). We found the ratio of time spent in the interaction zone in the habituation versus socialization phases was not significantly different versus controls (Fig. 4C). Instead, we found that *Chd4* cKOs exhibited decreased velocity throughout both the habituation and socialization phases of this test (Fig. 4D and E). This suggests that the environment of this particular test affected the cKO mice such that they were more hesitant to explore the testing arena—again suggesting an anxiety-related phenotype.

While *Chd4* cHTs spent equivalent time in the interaction zones versus controls (Fig. 4A), we found that they entered the large interaction zone around the stranger mouse significantly more frequently during the socialization period compared to wildtype, and not during the habituation phase (Fig. 4B). From this, we deduced that *Chd4* cHTs visit the stranger mouse more frequently but stay for briefer periods of time, which we later confirmed with video footage, suggesting a relatively subtle but nonetheless statistically significant alteration in social behavior.

To examine stereotyped and repetitive behaviors, we performed the marble burying test. Mice are introduced into a cage containing 20 marbles, and the number of marbles buried in a 30-min period is recorded. We found that *Chd4* cHTs buried significantly more marbles compared to controls (Fig. 4F), suggesting increased repetitive behaviors. By contrast, *Chd4* cKOs buried nearly all the marbles, or none at all. Overall, a statistically

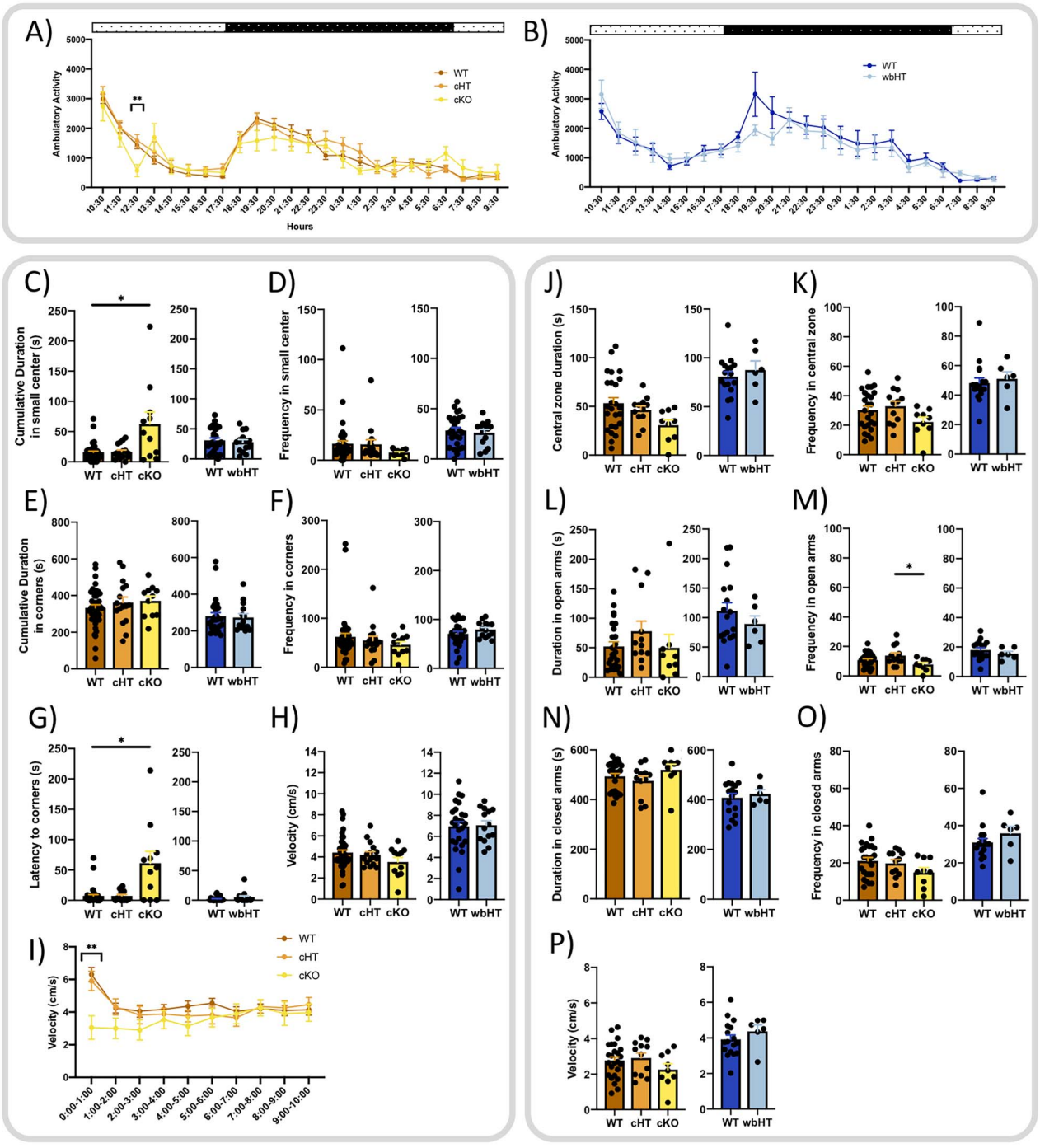

Figure 3. Exploration, activity levels, and anxiety behaviors in *Chd4* mutants. (A, B) Cumulative ambulatory activity counts per hour in the beam break assay for (A) wild-type (n = 28–41), cHT (n = 13–16), and cKOs (n = 7–11), or (B) wild-type (n = 26) and wbHTs (n = 14). Stippled bars indicate the light/dark cycle. (C–I) Open field test for wild-type (n = 41), cHT (n = 16), and cKOs (n = 11), or wild-type (n = 26) and wbHTs (n = 14) as indicated. Cumulative duration (C) and frequency (D) in the small center. Cumulative duration (E) and frequency (F) in the corners. Latency to reach the corners (G). Average velocity throughout the entire testing interval (H) or broken down into 1-min intervals (I). (J–P) Elevated plus maze test for wild-type (n = 25), cHT (n = 12), and cKOs (n = 9), or wild-type (n = 17) and wbHTs (n = 13) as indicated. Cumulative duration (J) and frequency (K) in the central zone. Cumulative duration (L) and frequency (M) in the open arms. Cumulative duration (N) and frequency (O) in closed arms. (P) Average velocity throughout the testing interval. Statistical analyses for wild-type, cHT, and cKO beam break are done via mixed effect analysis with Tukey's multiple comparison test post-hoc. Statistical analyses wild-type, cHT, and cKO velocity over time are done via two-way repeated measures ANOVA with Tukey-Kramer multiple comparison test post-hoc. All other statistical analyses for WT, cHT, and cKO comparisons are via one-way ANOVA with the Tukey-Kramer post-hoc test, with the exception of the cumulative duration in the small center (C) and latency to reach corners (G), which were instead analyzed via Kruskal-Wallis and Dunn's post-hoc test. Statistical analyses for wild-type and wbHT beam break are done via two-way repeated measures ANOVA with Sidak's multiple comparison test post-hoc. All other comparisons of wild-type vs. wbHT are via Student's t-test. See also Supplemental Data File for statistical summary. $^{*}p < 0.05$; $^{**}p < 0.01$.

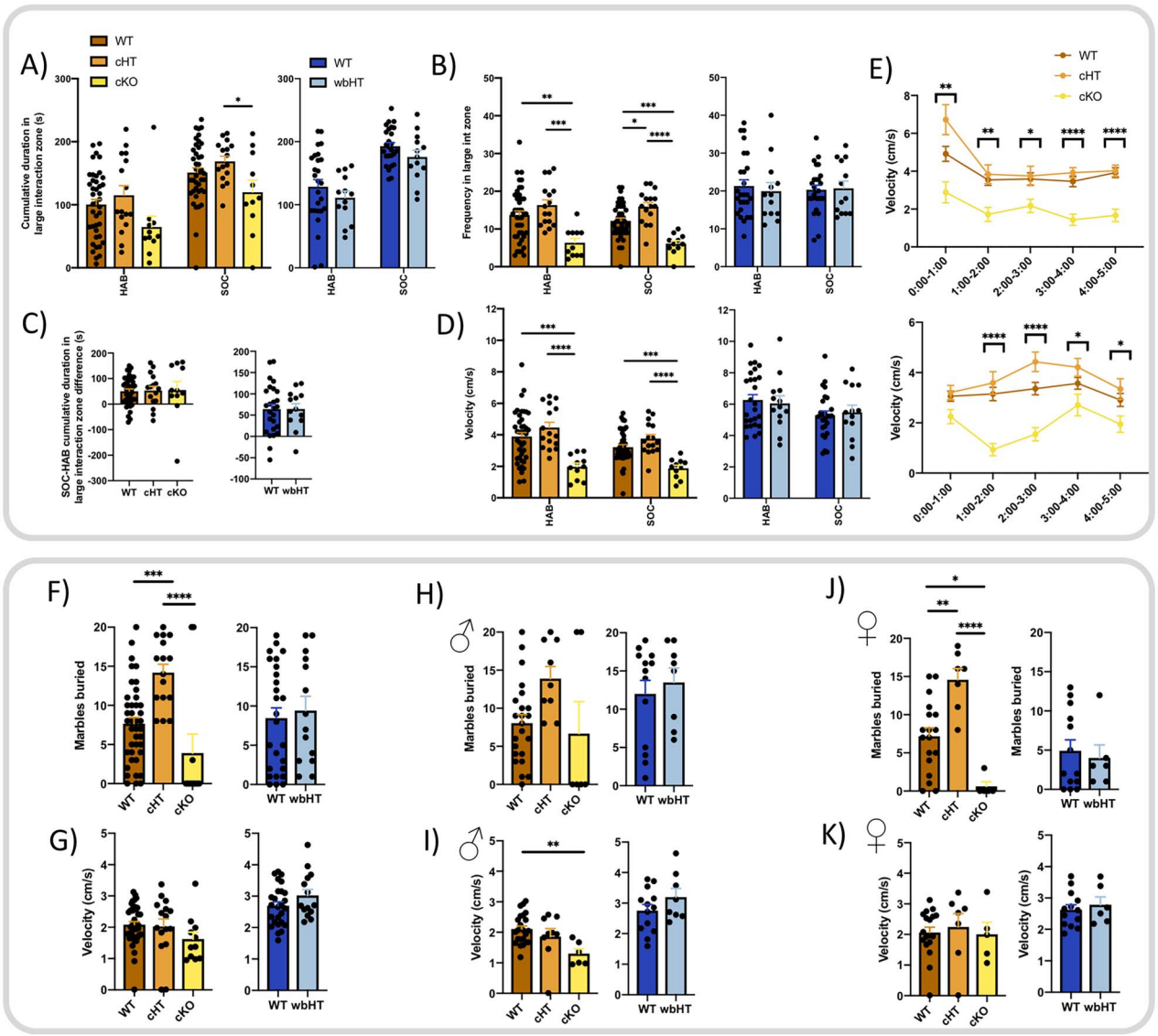

Figure 4. Sociability and repetitive behaviors in *Chd4* mutants. (A–D) Adult social interaction test, comparing the habituation phase (when the partner mice are absent) versus the socialization phase (when interaction partner mice are introduced into the chamber). Cumulative zonal duration (A), frequency (B), ratios of zonal duration (C), average velocity (D), and velocity broken down into 1-min intervals (E) for wild-type (n = 41), cHT (n = 16), and cKOs (n = 11), or wild-type (n = 26) and wbHTs (n = 13). (F–I) Marbles buried (F) and velocity (G) during the marble burying test for wild-type (n = 41), cHT (n = 16), and cKOs (n = 11), or wild-type (n = 26) and wbHTs (n = 14). (H–K) Shows the marble burying data shown in (F, G), but separated by males (H, I) and females (J, K). Wild-type (n = 23♂ and 18♀), cHT (n = 9♂ and 7♀), and cKO (n = 6♂ and 5♀) or wild-type (n = 13♂ and 13♀) and wbHT (n = 8♂ and 6♀). Statistical analyses for wild-type, cHT and cKO are via one-way ANOVA with Tukey–Kramer post-hoc test. Statistical analyses for wild-type and wbHT are via unpaired Student's t-test. $*p < 0.05$; $**p < 0.01$. Statistical analyses wild-type, cHT, and cKO velocity over time are done via two-way repeated measures ANOVA with Tukey's multiple comparison test post-hoc. See also Supplemental Data File for statistical summary.

significant decrease was observed (Fig. 4F). Interestingly, for both cHT and cKO animals, we found that the phenotype was more apparent in female animals (Fig. 4H and J). Taken together, the adult social interaction and marble burying tests reinforce the notion that *Chd4* cKOs exhibit elevated anxiety in specific environments, and implicate both cHTs and cKOs in repetitive behaviors. Despite the fact that wbHTs would be expected to capture all of the phenotypes exhibited by cHTs, we observed no social or repetitive behavioral phenotypes in wbHTs.

Whole-body *Chd4* heterozygotes exhibit sex-specific learning deficits

To examine learning and memory, we performed the Morris water maze test (Fig. 5A). Mice were trained over the course of 6 days to find a platform based on visual cues. On the 7th day (probe day) the platform was removed, which tests the ability of the mice to remember the platform's location. Neither *Chd4* cHTs or cKOs presented with significant changes in learning and memory during the test (Fig. 5B). When examined separately, males and females behaved equivalently (Fig. 5C and D). Fascinatingly, whereas *Chd4* wbHT mice did not demonstrate significant changes in activity, anxiety, repetitive, or social behaviors (Figs 3 and 4), they displayed significant deficits in learning and memory. From day 3 of the training phase onward, *Chd4* wbHT mice took longer to find the platform than wild-type control mice, suggesting a defect in learning (Fig. 5E). This was particularly evident in female wbHT mice (Fig. 5F and G). Additionally, female wbHTs had significantly decreased frequency of crossing the platform area on probe day,

suggesting a deficit in spatial memory (Fig. 5G). The probe day findings were further supported when we compared the amount of time mice spent in each quadrant of the pool. As expected, wild-type mice spent significantly more time in the platform quadrant (Fig. S9E) relative to all the others, while wbHTs spent equal amount of time in all quadrants of the pool (Fig. S9G). This suggests that wbHT females were unable to remember the platform's location based on visual cues.

To examine learning and memory using a different testing paradigm, we performed rotarod testing, which primarily assesses motor function, but can be used to address motor learning. Mice are placed upon a rotating rod that incrementally increases in speed (Fig. S10A). Over the course of repeated testing, mice learn to avoid falling from the rotarod. *Chd4* cHT and cKO mice did not exhibit any differences versus controls, nor did we observe any difference in male versus female performance (Fig. S10B and C). Likewise, we did not observe any defect in *Chd4* wbHT animals in the rotarod test when sexes were pooled (Fig. S10D). However, when sexes were separated, male wbHT mice did not show any phenotype on the rotarod, but female wbHTs exhibited impaired motor learning over the course of rotarod training (Fig. S10E). Since *Chd4* cHT animals do not exhibit corresponding phenotypes, these data indicate that female wbHTs exhibit learning deficits that map to neurodevelopmental events that fall outside of the *Emx1-Cre* expression window.

Discussion

NDDs are highly heterogeneous—both symptomatically and in terms of etiology. At the genetic level, chromatin remodellers represent a large proportion of the risk genes linked to these disorders, but the molecular mechanisms that link genotype to phenotype are not well understood. Despite a number of landmark studies examining *CHD4* in neurodevelopment, multiple gaps in our understanding of SIHIWES were unresolved. First, while *CHD4* mutations are clearly linked to both behavioral abnormalities and altered cortical growth, it remained unclear to what degree these phenotypes were linked. Indeed, while Chd4 protein is prominently expressed in dividing cortical progenitor cells, it is also expressed in postmitotic neurons and glia [24]. Second, while the observed macrocephalic and microcephalic phenotypes implicate *CHD4* in neocortical development, behavioral abnormalities could potentially map to other brain regions. Indeed, previous work in the murine cerebellum has already demonstrated that *Chd4* is required for behavior independently of effects on brain growth [13, 23]. Third, an important caveat is that previously reported *Chd4* mutant phenotypes manifested in cKOs rather than in heterozygotes. Since human *CHD4* mutations are exclusively heterozygous [15–17], it remains unclear to what degree these phenotypes actually reflect SIHIWES. A fourth related question is whether SIHIWES mutations are loss-of-function alleles, or pathological gain-of-function variants.

To begin to address these research gaps, we generated novel mouse models. Ablation of *Chd4* specifically in the developing telencephalon using the *Emx1-Cre* driver permitted survival of cKOs into adulthood, enabling the cortical knockout phenotype to be assessed postnatally for the first time. We predicted that constitutive versus conditional mutants would present with similar neurodevelopmental deficits that would differ only in severity. Instead, the observed phenotypes were categorically different—at both the neuroanatomical and behavioral levels. These results illustrate the pleiotropy of chromatin remodelling genes in neurodevelopment, and underscore the requirement for carefully matching genetic models to human NDD etiology.

Chd4 loss-of-function impairs cortical growth

Using the *Nestin-Cre* driver to generate *Chd4* cKOs, Nitarska *et al.* previously characterized defects in neocortical progenitor proliferation and apoptosis, culminating in perinatally lethality [24]. We obtained the same conditional *Chd4* allele used by Nitarska *et al.* (generated by the Katia Georgopoulos lab [21]), but instead utilized the *Emx1-Cre* driver, which is expressed in a later and more restricted fashion. We found that *Chd4* cKOs were viable into adulthood, albeit at reduced Mendelian frequencies. *Chd4* cKOs exhibited a prominent reduction in cortical size that was similar to that reported by the Riccio lab [24]. The observed microcephalic cKO phenotype also resembles growth impairments reported in other NuRD gene cKOs, including *Mbd3* or *Hdac1/2* [27, 28]. Biochemical data additionally suggest that Chd4 is particularly required in the context of the NuRD complex in embryonic cortical progenitor cells, when Chd3 and Chd5 are less expressed [24].

Surprisingly, despite the fact that cHTs and wbHTs are both hemizygous for *Chd4* throughout neocortical neurogenesis, wbHTs exhibited mild microcephalic phenotypes while cHTs were normal. The lack of analogous growth phenotypes in cHTs suggests that the requirement for *Chd4* during the neurogenetic developmental window is resilient to haploinsufficiency. Instead, the microcephalic phenotype in wbHTs likely arises due to cortex-extrinsic pathways, or from earlier neurodevelopmental functions. Indeed, in addition to its role in NuRD, Chd4 is also incorporated into the ChAHP complex [9]. ChAHP has been genetically implicated in early neurodevelopment, since *Adnp* knockout mice were reported to die at approximately E8.5 and exhibited defects in neural induction [29]. Similar effects were seen in pluripotent stem cell lines [9, 30, 31]. Moreover, *ADNP* is one of the most frequently mutated genes associated with ASD/ID [32, 33]. However, ASD has only been linked to one SIHIWES individual so far [16]. Future work will be required in order to clarify the contribution of NuRD and ChAHP chromatin remodelling complexes to neurodevelopment.

Although some SIHIWES patients have been reported to exhibit microcephaly [16], macrocephaly has been more frequently observed. Along with the Nitarska et al. study [24], our observations utilizing strong loss-of-function mutants argue that macrocephalic *CHD4* alleles likely act via dominant negative effects rather than via hemizygosity. In addition to *CHD4* itself [16], dominant negative effects have also been proposed to underlie neurodevelopmental disorders associated with NuRD complex genes, including *CHD5* [18], as well *GATAD2B* [34]. Perhaps accordingly, homozygous recessive mutations have been not previously associated with SIHIWES. Most SIHIWES alleles described to-date have been *de novo* missense pathogenic variants—usually located within the ATPase/helicase domains [15–17]. These variants likely generate enzymatically-inactive proteins that might nonetheless incorporate into chromatin remodelling complexes and bind regulatory elements in a non-productive manner.

Constitutive versus conditional mutations lead to divergent effects on behavior

We performed extensive behavioral testing in order to functionally validate our models. With respect to cognition, SIHIWES mutations are heterogeneous. For example, a pair of individuals harboring the same Arg1127Gln mutation had markedly different cognitive abilities. One individual exhibited moderate ID, and the other had IQ scores within the normal range [16]. Perhaps accordingly, we found that each *Chd4* mouse model presented with a

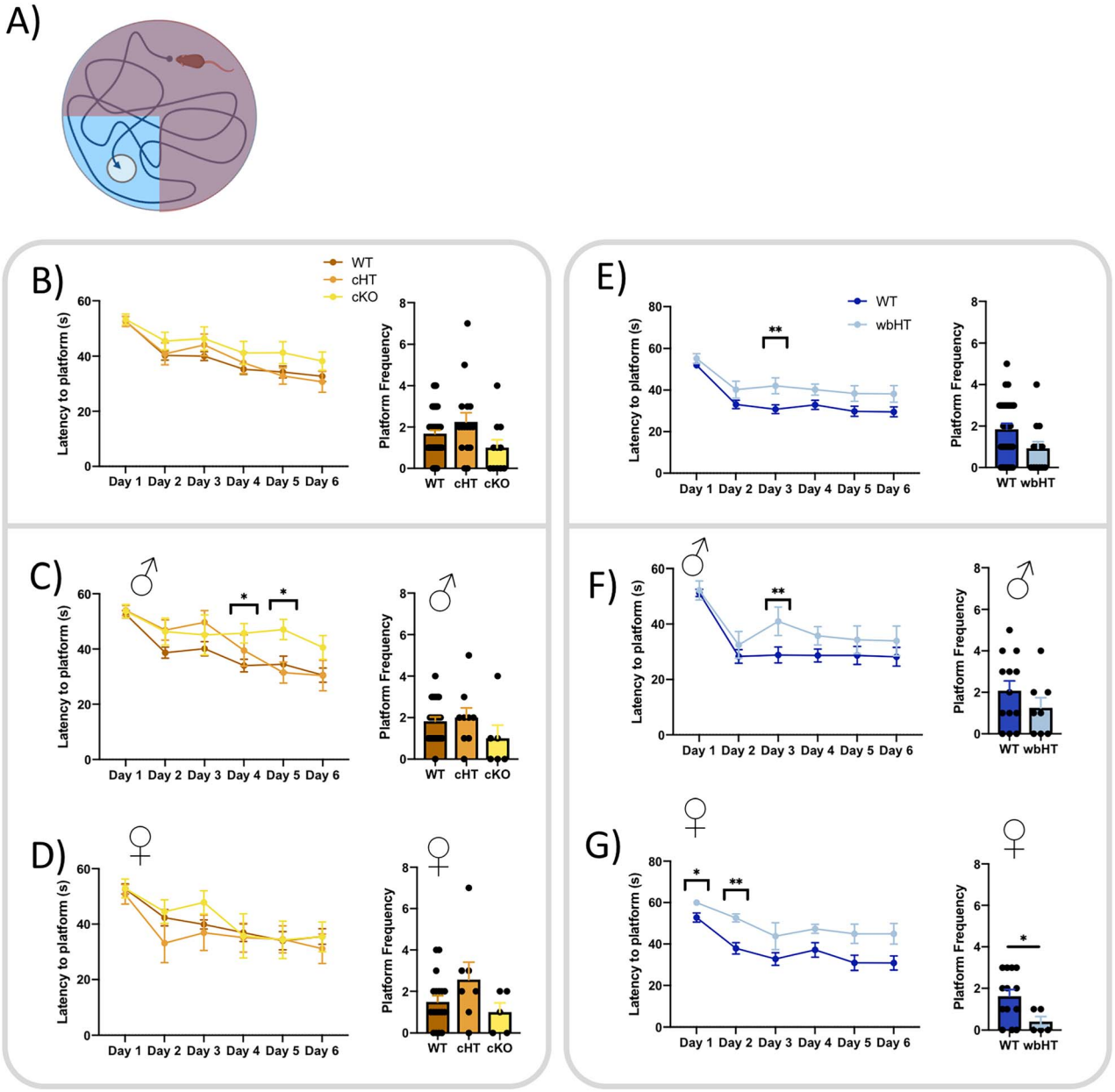

Figure 5. Sex-specific learning, memory, and growth deficits in *Chd4* wbHTs. (A) Schematic of Morris water maze test. (B–G) Latency to find the platform during training, and frequency to find the hidden platform on probe day in the Morris water maze test. (C, D, F, G) show the data shown in (B, E), but separated by sex. *Emx1-cre line*: wild-type (n = 23♂ and 18♀), cHT (n = 9♂ and 7♀), and cKO (n = 6♂ and 5♀). CMV-Cre line: wild-type (n = 13♂ and 13♀) or wbHT (n = 8♂ and 5♀). Statistical analyses for B–D are via two-way repeated measures ANOVA with Tukey-Kramer multiple comparison test post-hoc (latency) or one-way ANOVA with the Tukey-Kramer post-hoc test (platform frequency). Statistical analyses for E-G are via two-way repeated measures ANOVA with Sidak's multiple comparison test post-hoc (latency) or unpaired Student's t-test (platform frequency). See also Supplemental Data File for statistical summary. $^{*}p < 0.05$; $^{**}p < 0.01$.

different subset of behavioral defects, which are likely dependent on where and when *Chd4* expression is altered. Changes in repetitive behaviors and anxiety were affected only when the cortex was conditionally targeted, while changes in learning behaviors occurred only when the whole body was targeted—and only in female mice.

The connection between behavioral phenotypes and biological sex was unexpected. It is unclear why females would be more affected, though sex-specific changes in learning behaviors have previously been reported in other rodent NDD models [35, 36]. Female-specific phenotypes were mainly observed in wbHT mice and correlated with microcephaly. In humans, SIHIWES cases only include 12 females and 20 males, making it hard to draw conclusions regarding sex-specific differences. Males are generally diagnosed with NDDs more frequently than females, although this is partly attributable to the importance of X-linked genes within the genetic landscape of these disorders.

We tested animals for behavioral deficits that might be relevant to NDDs, but also examined animals for activity levels, sensory deficits, and motor system deficits. cHT, cKO, and wbHT mice exhibited intact optomotor reflexes, indicating normal visual function. All mutants exhibited equivalent circadian activity patterns that were not different versus controls. In most behavioral tests, *Chd4* mutants generally exhibited normal

velocities, although cKOs exhibited reduced velocity in the adult social interaction test. cKOs and wbHT females also exhibited deficits on the rotarod. These data suggest possible defects in sensorimotor function. cKOs and wbHTs also had slightly reduced body weight versus control animals, but we did not detect other obvious health defects in these animals, except that a subset of cKO adults developed skin lesions on their paws, which we believe may be due to *Emx1-Cre* expression in the limbs [25, 37]. We also observed hydrocephalus in several *Chd4* cKO animals. While hydrocephalus is linked to SIHIWES, the frequency of this observation was too low to determine whether it was truly linked to genotype. Moreover, we excluded hydrocephalic or significantly lesioned animals from our behavioral testing.

While cKO animals had the strongest anatomical and behavioral deficits, they likely fail to capture certain relevant phenotypes—such as deficits in spatial and motor learning. Despite the fact that wbHT animals have the most 'construct validity' in terms of their resemblance to SIHIWES mutations, behavioral deficits in these animals were relatively mild, and were confined only to female mice. Moreover, macrocephaly was not observed. Again, these data argue that SIHIWES mutations may not represent simple loss-of-function mutations. In the future, it will be important to generate mutants harboring patient-specific mutations in order to shed more light on pathogenic mechanisms and SIHIWES etiology.

Materials and Methods

Animal work

All animal work was approved by the University of Ottawa Animal Care Committee under ethical protocols OHRI-2856, OHRI-3155, and OHRI-3949, and was carried out following guidelines set out by the Canadian Council of Animal Care. The University of Ottawa Animal Care and Veterinary Services facility provided animal housing, where animals were kept in a 12-h light cycle with food and water provided *ad libitum*. *CMV-Cre* mice [26] were purchased directly from The Jackson Laboratory (*B6.C-Tg(CMV-cre)1Cgn/J*, Stock no. 006054). *Emx1-Cre+* mice [25] were generously donated by the David Picketts laboratory (OHRI, Ottawa, Canada). *Chd4*$^{fl/fl}$ founders were generously donated by the Katia Georgopoulos laboratory (Harvard, MA, USA). *Emx1-Cre* mice and *Chd4*$^{fl/fl}$ mice were backcrossed to C57BL/6J background mice a minimum of six generations before experimentation began. All wbHT animals were generated *de novo* from wild-type parents (i.e. *CMV-Cre+* crossed with *Chd4*$^{fl/+}$), in order to ensure that mutant phenotypes were not related to maternal effects or differences in rearing that might arise from mutant parents. Animals were genotyped using primer sets published in the referenced papers. In some cases, genotyping was further confirmed using Chd4 immunohistochemistry.

Immunofluorescence

Adult mice were euthanized via CO2 inhalation followed by cervical dislocation. The brains were dissected out, weighed, imaged, and fixed in 4% PFA overnight. Mouse pups were euthanized via decapitation, followed by brain dissection, imaging, fixing in 4% PFA overnight. Brains were subsequently transferred to 20% sucrose for 24 h, freezing solution (1:1 v/v of OCT:30% sucrose in PBS) for 24-36 h, and frozen down to −80°C in freezing solution.

Brains were sectioned coronally using a Leica CM1860 cryostat. Thickness was set at 14 μm for prenatal brains and 16 μm for postnatal brains. Sections were rinsed in 1× PBS followed by antigen retrieval in citrate buffer (10 mM Sodium citrate, 0.05% Tween 20, pH 6.0) using a pressure cooker for 10 min, and rinsing with water for 10 min. All antibodies were diluted in 30% w/v Bovine Serum Albumin, 0.4% Triton, and 1:5000 Hoechst in PBS. Primary antibodies were: rabbit anti-Aldh1l1 (1:100, Abcam ab87117), Rabbit anti-Brn2 (1:200, Cell Signaling Technology 12137S), mouse anti-Chd4 (1:200, Abcam ab70469), rabbit anti-Chd4 (1:100, Abcam ab72418), rat anti-Chd4 (1:100, BioLegend 942302), rat anti-Ctip2 (1:200, Abcam ab18465), rabbit anti-Neurog2 (1:250, Cell Signaling Technology 13144S), rabbit anti-Olig2 (1:200, Novus Biologicals NBP1-28667SS), mouse anti-Pax6 (1:10, Developmental Studies Hybridoma Bank PAX6), rabbit anti-Pax6 (1500; Novus NBP2–19711), rat anti-Satb2 (1100, Abcam ab51502), goat anti-Sox2 (1200, R&D Systems AF2018), rabbit anti-Tbr1 (1100, Cell Signaling Technology 49661), and rabbit anti-Tbr2 (1100, Abcam ab23345). Primary antibodies were incubated overnight at 4°C, followed by three 1X PBS washes, secondaries (Alexa Fluor 488 goat anti-mouse IgG (Jackson ImmunoResearch 115-545-003; 1:1000), DyLight 550 donkey anti-rat IgG (Invitrogen SA510027; 1:1000), Dylight 650 donkey anti-rabbit IgG (Novus Biologicals NBP1-75634; 1:1000)) for 1 h at room temperature, three 1× PBS washes and mounted in Mowiol mounting media (12% w/v Mowiol 4–88, 30% w/v glycerol, 120 mM Tris-Cl pH 8.5, 2.5% DABCO).

Cell counting and imaging

For consistency across coronal sections, the primary somatosensory cortex located between the crossing of the corpus collosum to the beginning of the hippocampus was targeted. Every other section, barring imperfections, was imaged using the Zeiss LSM900 Confocal Microscope at 200× magnification. Single Z-stack images were tiled and stitched using Zen software (Zeiss). Manual cell counting was performed using Adobe Photoshop on 200 μm-wide sections of somatosensory cortex between the crossing of the corpus callosum and the start of the hippocampus. Each 200 μm-wide section was separated into six 200 μm-wide bins of equal height for counting. This allowed the proportion of cells in the upper sixth area of the cortex to the lower sixth area of the cortex to be assessed, as well as total (i.e. absolute) counts. Three technical replicates were counted for each biological replicate (animal). For measurements of layer thickness, microscopic images of the somatosensory cortex (see above) were imported into Fiji and the 'Straight Line' tool was used to measure linear thickness in the radial axis using histological landmarks (white matter layer thickness: ependymal layer/subventricular zone to subplate; cortical thickness: subplate to pial surface). Three technical replicates were counted for each biological replicate (animal). Images were additionally processed using Photoshop, Powerpoint (Microsoft), and Biorender (Biorender.com).

Cortex and cerebellum area measurements

Brains were imaged post-dissection using a Zeiss Stemi 508 stereo microscope with Axiocam ERc 5 s at 6.3× magnification. Images were imported into Fiji and the outline of cortex or cerebellum was traced using the 'polygon selections' tool (see Fig. S2B and C). Area measurements were recorded and used for subsequent analysis. Scale was consistent across images and is depicted with arbitrary units.

Statistics

Data is presented as mean ± standard error of the mean unless otherwise indicated. Round black circles represent individual data points (animals). *Emx1-Cre* vs *CMV-Cre* lines were assessed separately due to significant differences between the control groups

of both lines. Statistical analysis was performed via Student's t-test, or one-way ANOVA with the Tukey-Kramer post-hoc test, as indicated in the text. $P < 0.05$ was considered statistically significant. ANOVA datasets were tested for equality of group variances using the Brown-Forsythe test. In cases where data failed to pass the Brown-Forsythe test, Kruskal-Wallis with Dunn's post-hoc test was used instead of one-way ANOVA. Statistical analyses for repeated measures over time were done via two-way repeated measures ANOVA, with Tukey's multiple comparison test (WT vs cHT vs cKO) or Sidak's multiple comparison test (WT vs wbHT) as indicated. Due to datapoints lost as a result of a software error, the WT vs cHT vs cKO beam-break test used a mixed effect analysis, wherein data were analyzed by fitting to a mixed model, instead of a two-way repeated measures ANOVA, which is incapable of handling the missing data points. All statistical analyses and graphs were performed/generated using GraphPad Prism version 8.0.0 for OS X, GraphPad Software, San Diego, California USA, www.graphpad.com. All statistical data is summarized in the Supplemental data file. All raw data will be made freely available upon request.

Behavior analysis

Behaviour testing, including protocols and materials provided, was performed through the Behavioural Core Facility at the University of Ottawa. All testing was performed blinded to animal genotypes. Mice were assessed between ~3–8 months of age, with females and males housed separately. Mice were habituated to the testing room for at least 30 min prior to testing commencing. Mice were handled (lifted out of cage and put back 3–4 times) for 5 days prior to commencing. Testing was scheduled so that mice only performed one behavior test a day following established protocols. Behavior testing was recorded with a video camera mounted appropriately and subsequently analyzed using Ethovision software (Noldus). Velocity and distanced travelled measurements were captured during each behavior test. During analysis, male and female data was pooled, unless otherwise indicated.

Elevated plus maze

Mice were placed in the middle of a plus shaped apparatus that was elevated above the ground for 10 min under 100 lux lighting. Two arms of the plus maze, opposite to each other, were enclosed (6 cm wide × ~69 cm long, 20 cm high walls) while the remaining two were open (6 cm wide × ~69 cm long, raised 74 cm off the floor). The number of entries the mouse made into the closed versus open arms, as well as the time spent in the closed versus open arms was measured. Measurements of mice activity, videos of mice activity, and analysis was collected using Ethovision software (Noldus).

Open field

Mice were placed in the middle of an opaque plastic box (45 cm × 45 cm × 45 cm) with an open top. A camera mounted above the box recorded the mice activity for 10 min under 300 lux light. Ethovision software (Noldus) was used to analyze videos of mice activity. The amount of time a mice spent in the center of the box (small centre and large centre) and the corners of the box was recorded. The latency for the mice to reach the corners of the box was also measured.

Beam break

Mice were placed in a new housing cage that was placed between a photocell emitters and photocell receptors system for 24 h. Disruption of the infrared light as the mouse moved through the cage was detected and recorded by the photocell analyzer (Micromax Analyzer, AccuScan) and subsequently tallied through computer analysis (Fusion 5.3 software, Omnitech Electronics Inc.). Ambulatory Activity Counts, measuring the amount of beam breaks that occurred while the animal was ambulating (vs stereotypic behaviour such as grooming, etc.) was plotted. Due to a software malfunction, data was lost during the first 3 to 4 h of testing for one cohort of mice, which included 13 WTs, 3 *Chd4* cHTs and 4 *Chd4* cKOs. The remaining data was added at 12:30–13:30.

Marble burying

Mice were first habituated to the testing arena with no marbles present for 5 min. Subsequently, 20 marbles were evenly spaced atop woodchip bedding in a 4 × 5 marble grid in the arena. Mice were placed in the testing area again for 30 min and the number of marbles buried after this time was manually recorded. 75%+ of marbled covered by bedding was considered as buried.

Adult social interaction

Mice were habituated in red light before testing, and the test was subsequently performed under red light. During the habituation phase, a mouse was placed in the corner of a 45 cm × 45 cm × 45 cm box with a 5.5 cm × 9.6 cm wire mesh rectangular cage located along one side and allowed to explore for 5 min. After this point, the mouse was removed and temporarily placed in a clean container for 5 min. Next, a C57BL/6J background social target mouse (of the same gender and of similar age) was placed inside the wire mesh cage for the socialization phase. The tested mouse was reintroduced into the box for 5 min and activity recorded. Time spent and number of entries of the mouse's body near the cage (large interaction zone) and in the corners was recorded, as well as time and number of entries the nose point of the mouse entered the small interaction zone around the cage.

Rotarod

Mice were placed on a horizontal textured rod (IITC Life Science, Ugo Basile) rotating at a speed of 5 RPM. The speed was gradually increased to 40 RPM over the course of 5 min and the time the mouse spent on the rod before falling off (latency to fall) was recorded. Mice were trained on the Rotarod four times a day with a 10 min intertrial interval in their home cage. This was performed for four consecutive days.

Morris water maze

A ~132 cm diameter pooled was filled with opaque (white non-toxic tempura paint) water (22°C) with a 10 cm diameter white platform hidden 1 cm below the surface of the water. The pool had 4 starting locations at the edge of the pool located equidistant to each other, and the platform was located between two of them about 24 cm from the edge of the pool. Lighting was set to 140 lux and the pool was surrounded by 4 white 'walls'. Two black visual cues were located on two of the adjacent walls to allow for spatial navigation. Briefly, a mouse was placed in the water at one of the starting points and allowed to try and find the platform for 1 min. If they did not find it, the platform was tapped by the researcher, and if the mice still did not find it, gently guided by the tail towards the platform. Once on the platform, the mouse was left for 10 s, prior to being removed, toweled off and returned to its home cage for a 15-min intertrial interval. Mice were trained 4 times a day at each of the locations, the order of which was randomized. After 6 days of training, the platform was removed and the amount of time the mouse spent in the quadrant where

the platform was located, and the number of times the mouse crossed the area where the platform had been was measured.

Optomotor analysis

The StriaTech Optodrum was used to assess visual acuity in mice. Briefly, a mouse was placed atop a white 9 cm diameter platform in the middle of the OptoDrum (box shaped). Contrast cycles was set at 99.72% with a constant rotation speed of 12°/s. The number of cycles was set to start at 60 cycles (0.167 cyc/°) and increased/decreased following an automatic staircase procedure that allowed determination of visual acuity (i.e. max number of cycles mice would respond to). Mice were tested three times in one day and the mean of these trials was calculated and graphed.

Acknowledgements

We are indebted to Katia Georgopoulos for previously sharing *Chd4*^{fl} mice, and to David Picketts for sharing *Emx1-cre* mice. We are grateful to Kerstin Ure, Sarah Kealey, and Katherine Tacay from the uOttawa *Animal Behaviour Core*, for their help with behavior testing. We also thank *Animal Care and Veterinary Service*, and *Cell Biology and Image Acquisition* core facilities. We thank Samuel Clémot-Dupont, Ida Malloy, and Mattar lab members for their ongoing help and input. We thank Diane Lagace, David Picketts, and Jing Wang for their advice and guidance.

Author contributions

Conceptualization: S.L., P.M. Data curation: S.L., P.M. Formal analysis: all authors. Investigation: all authors. Project administration, resources, supervision: P.M. Visualization: S.L., P.M. Writing—original draft: S.L., P.M. Writing, review, and editing: all authors.

Supplementary data

Supplementary data is available at *HMG Journal* online.

Conflict of interest statement: The authors declare no conflicts of interest.

Funding

This project was supported by the Canadian Institutes of Health Research (CIHR) Operating Grants PJT-166032 and PJT-166074. Confocal microscopy was supported by an infrastructure grant from the Canada Foundation for Innovation (JELF 37688 to P.M.). The Mattar lab also acknowledges generous support from the Simon's Foundation for Autism Research Initiative (SFARI Pilot Award 609562) as well as the Brain & Behavior Research Foundation (NARSAD Young Investigator Award from 28564). S.L. was supported by graduate scholarships from the Natural Sciences and Engineering Research Council of Canada (NSERC), as well as the Ontario Graduate Scholarship. P.M. currently holds the Gladys and Lorna J. Wood Chair for Research in Vision.

References

1. Clapier CR, Iwasa J, Cairns BR. *et al.* Mechanisms of action and regulation of ATP-dependent chromatin-remodelling complexes. *Nat Rev Mol Cell Biol* 2017;**18**:407–22.
2. Bjornsson HT. The Mendelian disorders of the epigenetic machinery. *Genome Res* 2015;**25**:1473–81.
3. Goodwin LR, Picketts DJ. The role of ISWI chromatin remodeling complexes in brain development and neurodevelopmental disorders. *Mol Cell Neurosci* 2018;**87**:55–64.
4. Sokpor G, Castro-Hernandez R, Rosenbusch J. *et al.* ATP-dependent chromatin remodeling during cortical neurogenesis. *Front Neurosci* 2018;**12**:226.
5. Larrigan S, Shah S, Fernandes A. *et al.* Chromatin remodeling in the brain-a NuRDevelopmental Odyssey. *Int J Mol Sci* 2021;**22**:4768.
6. Wade PA, Gegonne A, Jones PL. *et al.* Mi-2 complex couples DNA methylation to chromatin remodelling and histone deacetylation. *Nat Genet* 1999;**23**:62–6.
7. Xue Y, Wong J, Moreno GT. *et al.* NURD, a novel complex with both ATP-dependent chromatin-remodeling and histone deacetylase activities. *Mol Cell* 1998;**2**:851–61.
8. Zhang Y, LeRoy G, Seelig HP. *et al.* The dermatomyositis-specific autoantigen Mi2 is a component of a complex containing histone deacetylase and nucleosome remodeling activities. *Cell* 1998;**95**:279–89.
9. Ostapcuk V, Mohn F, Carl SH. *et al.* Activity-dependent neuroprotective protein recruits HP1 and CHD4 to control lineage-specifying genes. *Nature* 2018;**557**:739–43.
10. Bornelov S, Reynolds N, Xenophontos M. *et al.* The nucleosome remodeling and deacetylation complex modulates chromatin structure at sites of active transcription to fine-tune gene expression. *Mol Cell* 2018;**71**:56–72.e4.
11. Kaaij LJT, Mohn F, van der Weide RH. *et al.* The ChAHP complex counteracts chromatin looping at CTCF sites that emerged from SINE expansions in mouse. *Cell* 2019;**178**:1437–1451 e1414.
12. Thorn GJ, Clarkson CT, Rademacher A. *et al.* DNA sequence-dependent formation of heterochromatin nanodomains. *Nat Commun* 2022;**13**:1861.
13. Yamada T, Yang Y, Hemberg M. *et al.* Promoter decommissioning by the NuRD chromatin remodeling complex triggers synaptic connectivity in the mammalian brain. *Neuron* 2014;**83**:122–34.
14. Yoshida T, Hu Y, Zhang Z. *et al.* Chromatin restriction by the nucleosome remodeler Mi-2beta and functional interplay with lineage-specific transcription regulators control B-cell differentiation. *Genes Dev* 2019;**33**:763–81.
15. Sifrim A, Hitz MP, Wilsdon A. *et al.* Distinct genetic architectures for syndromic and nonsyndromic congenital heart defects identified by exome sequencing. *Nat Genet* 2016;**48**:1060–5.
16. Weiss K, Lazar HP, Kurolap A. *et al.* The CHD4-related syndrome: a comprehensive investigation of the clinical spectrum, genotype-phenotype correlations, and molecular basis. *Genet Med* 2020;**22**:389–97.
17. Weiss K, Terhal PA, Cohen L. *et al.* De novo mutations in CHD4, an ATP-dependent chromatin remodeler gene, cause an intellectual disability syndrome with distinctive dysmorphisms. *Am J Hum Genet* 2016;**99**:934–41.
18. Parenti I, Lehalle D, Nava C. *et al.* Missense and truncating variants in CHD5 in a dominant neurodevelopmental disorder with intellectual disability, behavioral disturbances, and epilepsy. *Hum Genet* 2021;**140**:1109–20.
19. Snijders Blok L, Rousseau J, Twist J. *et al.* CHD3 helicase domain mutations cause a neurodevelopmental syndrome with macrocephaly and impaired speech and language. *Nat Commun* 2018;**9**:4619.
20. O'Shaughnessy-Kirwan A, Signolet J, Costello I. *et al.* Constraint of gene expression by the chromatin remodelling protein CHD4 facilitates lineage specification. *Development* 2015;**142**:2586–97.
21. Williams CJ, Naito T, Arco PG. *et al.* The chromatin remodeler Mi-2beta is required for CD4 expression and T cell development. *Immunity* 2004;**20**:719–33.

22. Goodman JV, Yamada T, Yang Y. *et al.* The chromatin remodeling enzyme Chd4 regulates genome architecture in the mouse brain. *Nat Commun* 2020;**11**:3419.
23. Yang Y, Yamada T, Hill KK. *et al.* Chromatin remodeling inactivates activity genes and regulates neural coding. *Science* 2016;**353**:300–5.
24. Nitarska J, Smith JG, Sherlock WT. *et al.* A functional switch of NuRD chromatin remodeling complex subunits regulates mouse cortical development. *Cell Rep* 2016;**17**:1683–98.
25. Gorski JA, Talley T, Qiu M. *et al.* Cortical excitatory neurons and glia, but not GABAergic neurons, are produced in the Emx1-expressing lineage. *J Neurosci* 2002;**22**:6309–14.
26. Schwenk F, Baron U, Rajewsky K. A cre-transgenic mouse strain for the ubiquitous deletion of loxP-flanked gene segments including deletion in germ cells. *Nucleic Acids Res* 1995;**23**:5080–1.
27. Knock E, Pereira J, Lombard PD. *et al.* The methyl binding domain 3/nucleosome remodelling and deacetylase complex regulates neural cell fate determination and terminal differentiation in the cerebral cortex. *Neural Dev* 2015;**10**:13.
28. Montgomery RL, Hsieh J, Barbosa AC. *et al.* Histone deacetylases 1 and 2 control the progression of neural precursors to neurons during brain development. *Proc Natl Acad Sci U S A* 2009;**106**:7876–81.
29. Pinhasov A, Mandel S, Torchinsky A. *et al.* Activity-dependent neuroprotective protein: a novel gene essential for brain formation. *Brain Res Dev Brain Res* 2003;**144**:83–90.
30. Sun X, Yu W, Li L. *et al.* ADNP controls gene expression through local chromatin architecture by association with BRG1 and CHD4. *Front Cell Dev Biol* 2020;**8**:553.
31. Yan Q, Wulfridge P, Doherty J. *et al.* Proximity labeling identifies a repertoire of site-specific R-loop modulators. *Nat Commun* 2022;**13**:53.
32. Helsmoortel C, Vulto-van Silfhout AT, Coe BP. *et al.* A SWI/SNF-related autism syndrome caused by de novo mutations in ADNP. *Nat Genet* 2014;**46**:380–4.
33. Satterstrom FK, Kosmicki JA, Wang J. *et al.* Large-scale exome sequencing study implicates both developmental and functional changes in the neurobiology of autism. *Cell* 2020;**180**:568–584 e523.
34. Shieh C, Jones N, Vanle B. *et al.* GATAD2B-associated neurodevelopmental disorder (GAND): clinical and molecular insights into a NuRD-related disorder. *Genet Med* 2020;**22**:878–88.
35. Ghahremani R, Mohammadkhani R, Salehi I. *et al.* Sex differences in spatial learning and memory in valproic acid rat model of autism: possible beneficial role of exercise interventions. *Front Behav Neurosci* 2022;**16**:869792.
36. Yang M, Bozdagi O, Scattoni ML. *et al.* Reduced excitatory neurotransmission and mild autism-relevant phenotypes in adolescent Shank 3 null mutant mice. *J Neurosci* 2012;**32**:6525–41.
37. Shibata S, Kashiwagi M, Morgan BA. *et al.* Functional interactions between Mi-2beta and AP1 complexes control response and recovery from skin barrier disruption. *J Exp Med* 2020;**217**:jem.20182402.